LAWRENCE
LIVERMORE
NATIONAL
LABORATORY

LLNL-JRNL-403423

Ion spatial distributions at the liquid-vapor interface of aqueous potassium fluoride solutions

M. A. Brown, R. D'Auria, I-F. W. Kuo, M. J. Krisch, D. E. Starr, H. Bluhm, D. J. Tobias, J. C. Hemminger

May 2, 2008

Physical Chemistry Chemical Physics

Disclaimer

04/22/2008

Ion spatial distributions at the liquid-vapor interface of aqueous potassium fluoride solutions

Matthew A. Brown,[1] Raffaella D'Auria,[1] I-F. William Kuo,[2] Maria J. Krisch,[1] David E. Starr,[3†] Hendrik Bluhm,[3] Douglas J. Tobias,[1,*] John C. Hemminger[1,*]

1. Department of Chemistry and Air UCI, University of California, Irvine, Irvine, California 92697
2. Chemical Sciences Division, Lawrence Livermore National Laboratory, Livermore, California 94551
3. Chemical Sciences Division, Lawrence Berkeley National Laboratory, Berkeley California 94720

Author e-mail addresses:

Matthew A. Brown: mabrown@uci.edu

Raffaella D'Auria: rdauria@uci.edu

I-F. William Kuo: kuo2@llnl.gov

Maria J. Krisch: mkrisch@uci.edu

David E. Starr: destarr@lbl.gov

Hendrik Bluhm: hbluhm@lbl.gov

Douglas J. Tobias: dtobias@uci.edu

John C. Hemminger: jchemmin@uci.edu

[*] To whom correspondence should be addressed

[†] Present address: Center for Functional Nanomaterials, Brookhaven National Laboratory, Upton, New York 11973.

Summary

X-ray photoemission spectroscopy operating under ambient pressure conditions is used to probe ion distributions throughout the interfacial region of a free-flowing aqueous liquid micro-jet of 6 M potassium fluoride. Varying the energy of the ejected photoelectrons by carrying out experiments as a function of x-ray wavelength measures the composition of the aqueous-vapor interfacial region at various depths. The F^- to K^+ atomic ratio is equal to unity throughout the interfacial region to a depth of 2 nm. The experimental ion profiles are compared with the results of a classical molecular dynamics simulation of a 6 M aqueous KF solution employing polarizable potentials. The experimental results are in qualitative agreement with the simulations when integrated over an exponentially decaying probe depth characteristic of an APPES experiment. First principles molecular dynamics simulations have been used to calculate the potential of mean force for moving a fluoride anion across the air-water interface. The results show that the fluoride anion is repelled from the interface, and this is consistent with the depletion of F^- at the interface revealed by the APPES experiment and polarizable force field-based molecular dynamics simulation. Together, the APPES and MD simulation data provide a detailed description of the aqueous-vapor interface of alkali fluoride systems. This work offers the first direct observation of the ion distribution at a potassium fluoride aqueous solution interface. The current experimental results are compared to those previously obtained for saturated solutions of KBr and KI to underscore the strong difference in surface propensity between soft/large and hard/small halide ions in aqueous solution.

Introduction: Our understanding of ion distributions at the liquid-vapor interface of electrolyte solutions has been fundamentally altered by recent experimental and computational results, briefly reviewed in what follows. Davidovits and coworkers[1] first suggested that increased halide ion concentrations at the interface of NaBr and NaI solutions could account for their measured reactive uptake coefficients of gas-phase $Br_{2(g)}$ and $Cl_{2(g)}$. Their observations could not be explained solely by traditional bulk phase aqueous chemistry, and suggested that halide anions are present on the surfaces of the solutions. The first theoretical predictions of the presence of halide anions on the surface of small water clusters came from molecular dynamics (MD) simulations by Dang et al.[2] and Perera and Berkowitz.[3] In these simulations, a force field that explicitly accounted for electronic polarization was required to produce configurations in which the anions were located on the cluster surface. Using essentially the same force fields, Jungwirth and Tobias[4, 5] (JT) predicted that halide anions also adsorb to the extended interface of bulk solutions, thereby challenging the traditional model of an electrolyte interface as being devoid of ions.

The MD simulations of JT predict an increased halide ion concentration in the interfacial region of aqueous alkali iodide and bromide solutions relative to their respective bulk concentrations, with the surface affinity for the interface following the Hofmeister series.[6-8] In contrast with the predicted surface enhancement of the heavier halides, JT's MD simulation of sodium fluoride agrees with the traditional point ion model of an electrolyte solution, in which no preferential surface segregation of ions exists at the interface, and both the anions and cations are repelled from the interface.[6] Figure 1 shows snapshots (side view) and the density profiles from the MD simulations of JT for 1.2 molar sodium halide salt solutions. Here, $\rho(z)$ is the depth-dependent density at a distance z from the center of the simulated slab and ρ_o refers to the bulk concentration. In the near surface region the heavier halide ions (I^- and Br^-) have densities ($\rho(z)/\rho_o$) greater than that of the bulk. Deeper in the solution the cation concentration is enhanced and the halide ion concentration depleted, creating an electric double layer below which the MD simulations predict that both the halide and sodium ions tend smoothly to their bulk concentration. The case is strikingly different for the density profiles of the sodium fluoride solution in which neither ion shows preferential surface

enhancement at the aqueous-vapor interface. In this case both the ions are predicted to reside below the Gibbs dividing surface (not shown in the figure), the ideal surface at which the surface excess of the solvent is zero.

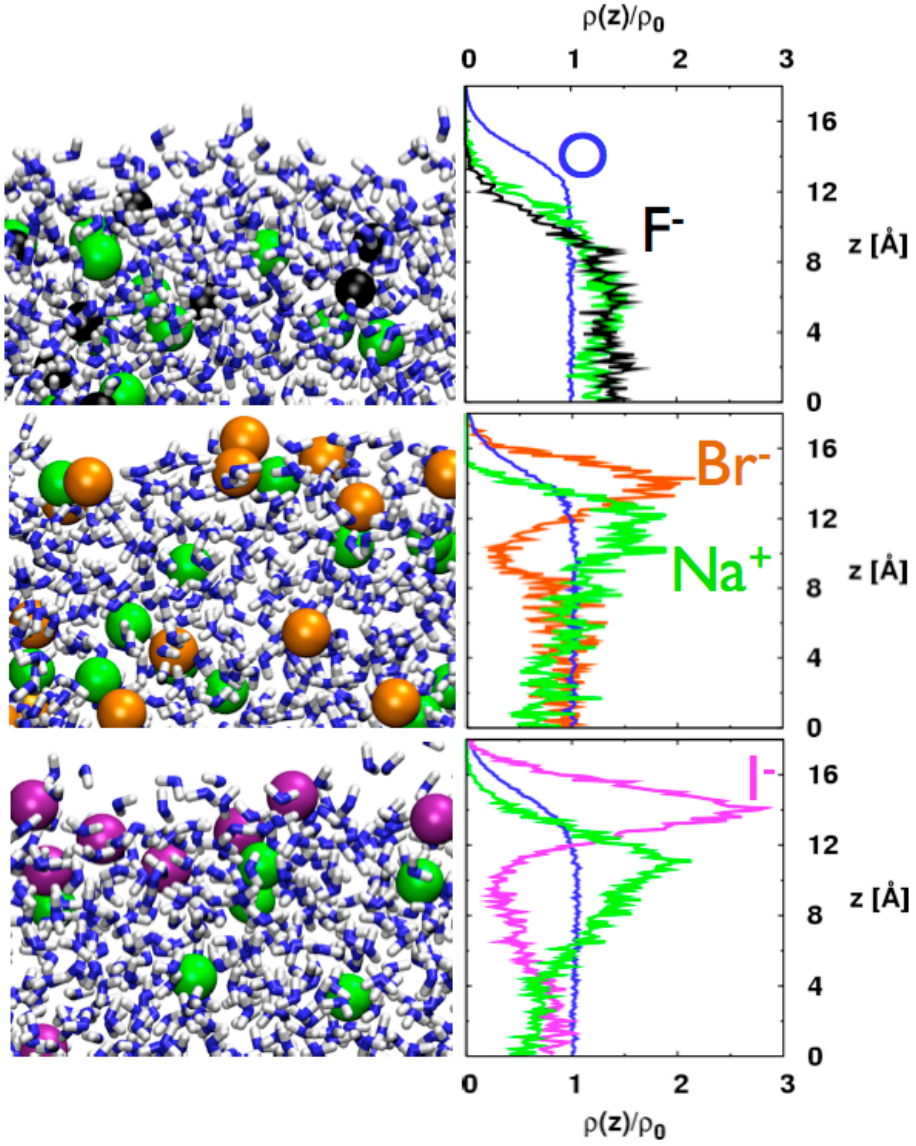

Figure 1: Snapshots (side view) of the solution/air interface of 1.2 M aqueous sodium halides and density profiles (number densities) of water oxygen atoms and ions plotted vs. distance from the center of the slabs in the direction normal to the interface, normalized by the bulk water density. From top to bottom the systems are NaF, NaBr, and NaI. The colors of the density profiles correspond to the coloring of the atoms in the snapshots (blue for water and green for Na^+ in all of the plots, black for F^-, orange for Br^-, and magenta for I^-). The water density is scaled differently from those of the ions so that it can be easily displayed on the same plots.[6]

The computational results of JT motivated several subsequent experimental efforts to study of the interfacial properties of electrolyte solutions. A particular early

emphasis was placed on confirming the predicted surface enhancement of the larger and more polarizable anions in the near surface region of ionic solutions. Until recently, however, direct experimental corroboration of the computational models of JT proved to be very challenging due to the experimental limitations and difficulties of measuring molecular structure and/or composition at the aqueous-vapor interface.

In spite of these difficulties there have been several studies focused on ion distributions and water structure in solution. Using photoelectron spectroscopy Winter and coworkers[9, 10] have shown that the electronic binding energies of solvated anions and cations are independent of salt concentration, and the surface propensity of I^- in dilute solutions of aqueous tetrabutylammonium iodide (TBAI). Resonant second harmonic generation (SHG) studies by Saykally and coworkers[11-14] revealed increased anion concentrations at the free surface of many salt solutions when the results are fit with a Langmuir adsorption model. Studies employing vibrational sum-frequency generation (VSFG) have also characterized the interfacial region of alkali halide solutions.[15, 16] Based on changes in the hydrogen-bonding network of liquid water at the interface of alkali halide solutions, Liu et al.[15] report increased interfacial concentrations of both I^- and Br^-, while Raymond and Richmond[16] report decreased (albeit non-vanishing) iodide, bromide and chloride ion concentrations at the interface relative to that of the bulk. Finally, ambient pressure x-ray photoemission studies of concentrated iodide and bromide solutions have provided the most direct experimental evidence of ion profiles throughout the interfacial region. Specifically, Ghosal et al.[17] have confirmed increased halide ion concentrations throughout the aqueous-vapor interfacial region of concentrated I^- and Br^- electrolytic solutions, while also experimentally validating the increased propensity of the iodide anion over the bromide anion for the interface. These results are in excellent agreement with the MD simulations of JT.

To date there have been fewer experimental studies that have focused on the distribution of fluoride ions throughout the interfacial region. Among the few recent studies, the liquid-vapor interface of aqueous alkali fluoride systems has been explored by Allen and coworkers[15] and Richmond and coworkers[16] in the two independent VSFG studies[15, 16] already mentioned. Owing to the nature of the VSFG experimental technique, ion concentrations are not directly probed, so conclusions regarding the presence/absence

of ions at the interface are drawn from examination of the changes in the hydrogen-bonding network of water in the presence of NaF. The conclusions reached in these investigations are somewhat different: Allen and co-workers[15] report that the interfacial water structure of a NaF electrolyte solution is similar to that of neat water, while Richmond and co-workers[16] conclude that F^- exhibits structure making characteristics in electrolyte solution, thus implying a decreased interfacial ion concentration. Clearly, additional experiments are necessary to characterize the distribution of fluoride ions throughout the aqueous-vapor interfacial region.

Herein, the interfacial ion concentrations of a free-flowing liquid micro-jet of 6 molar aqueous KF is characterized as a function of probe depth into the solution using ambient pressure photoemission spectroscopy (APPES). Under these experimental conditions the liquid jet is in equilibrium with its vapor pressure allowing the measurement of equilibrated ion profiles. The experimental results are compared with the results of a classical MD simulation of a concentrated KF aqueous solution employing polarizable potentials, and a first principles MD calculation of the potential of mean force for translocating an F^- ion across the air-water interface. Both the experiments and simulation agree that the fluoride anion does not have a propensity for the aqueous-vapor interface. The current results are compared with previous studies of interfacial ion profiles in saturated solutions of KBr and KI.[17]

Results and Discussion: Figure 2 presents XP spectra of the F(1s), K(2p) and O(1s) core levels for a 6 molar solution of KF at 150 eV photoelectron kinetic energy (PKE). A small amount of sample charging (~2 eV) was observed during data acquisition, and the binding energies of the F(1s) and K(2p) atomic orbitals shown in Figure 2 have been charge corrected to the values reported by Morgan et al.[18] for a dry KF salt. There are two peaks in the spectra of the O(1s) region (Figure 2c) with the lower binding energy peak at ~535 eV assigned to the surface water signal of the liquid micro-jet and the higher binding energy peak at ~537 eV assigned as the gas phase O(1s) signal of the background water vapor. One advantage of using the liquid micro-jet as a clean, continuously renewable sample surface is seen in Figure 2b. The core 1s binding energy of aliphatic carbon is shifted to lower binding energies by 8 eV relative to that of $K(2p_{3/2})$ and it is evident from the spectrum in Figure 2b that this system is free from any aliphatic

carbon impurities. This is the first time that our liquid salt solutions have been devoid of adventitious carbon impurities under ambient pressure conditions.

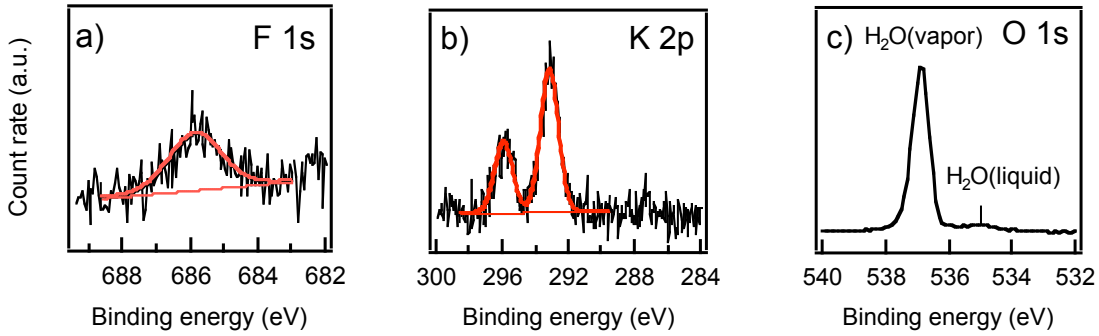

Figure 2: Collected APPES spectra from the 6 molar potassium fluoride solution at 150 eV kinetic energy. (a); F(1s) region (b); K(2p) and C(1s) regions (c); O(1s) region. There are two peaks in the O(1s) region of the spectra. The peak at 537 eV is assigned as the gas phase signal of the background water vapor while the peak at 535 eV is the surface water signal of the liquid micro-jet.

The probe depth in an XPS experiment is determined by the inelastic scattering of the photoelectrons as they exit the sample. By carrying out experiments as a function of x-ray wavelength, the concentration of different ions in solution can be directly interrogated for a specific volume element, which generates a density profile of ions into solution. Experimental values of electron mean escape depth (related to the inelastic mean free path (IMFP) through a geometrical correction factor) for neat liquid water have been reported by Ottosson[19] over an energy range of 70-900 eV. A minimum is observed for photoelectrons of 150 eV, with a nearly linear increase towards higher PKE. The depth dependence of the IMFP in liquids allows experiments to be carried out over varying probe depths. Depth profiling provides a distinct advantage not available through second-order optical processes (which are limited to a single probe depth for a given solution)[20, 21] and allows for comparison between the XPS experimental density profiles and those obtained by classical MD simulations. Ghosal et al.[17] have previously shown that the ion profiles obtained by multi-depth profiling using APPES for saturated solutions of potassium iodide and bromide (KI and KBr) are in qualitative agreement with the classical MD simulations of JT.

For each spectrum shown in Figure 2, peaks are fit and normalized as described above to obtain the relative concentration of each ion at the liquid-vapor interface. The

circles in Figure 3 show the resulting fluoride to potassium atomic ratio as a function of PKE and estimated probe depth, z, below the liquid-vapor interface. The measured results show a slight increase in the F^- to K^+ atomic ratio as the sample probe depth is increased; however the slight increase is within the present precision of our measurements. The anion/cation atomic ratio of a 6 M KF aqueous solution remains unity throughout the interfacial region. These results provide the first experimental measurements of the anion/cation atomic ratio throughout the interfacial region of an alkali fluoride electrolyte solution to a probe depth of 2 nm.

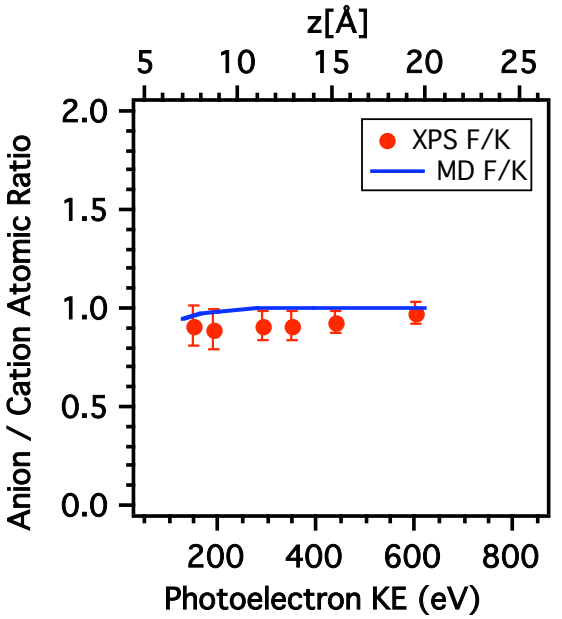

Figure 3: The measured and predicted anion/cation atomic ratios as a function of photoelectron kinetic energy. The circles are the experimental results while the solid line is the atomic ratio calculated from the MD simulation. Varying the energy of the emitted photoelectrons collects a multi-depth profile into solution. The predicted atomic ratio is calculated by integration of a convolution integral for each ion, where the IMFP values of Ottosson were used.[19]

The density profiles computed from the MD simulation of a 6 M aqueous KF solution are shown in Figure 4. The normalized area of the ion density profiles (potassium shown in red and fluoride in black) are set equal, and the water density (shown in blue) has been scaled to fit within the limits of the figure. The ions are repelled from the interface in accordance with the classical interpretation of a negative surface excess characteristic of alkali-halide aqueous solutions.

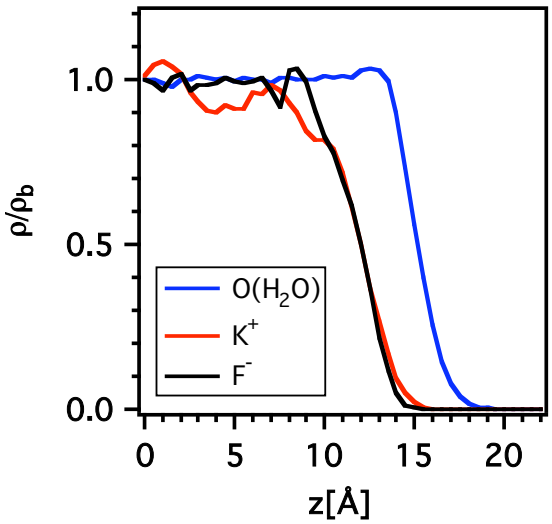

Figure 4: Density profiles for a 6 M aqueous solution of KF. The oxygen from the water molecules is shown in blue, potassium and fluoride ions in red and black respectively. The water density has been scaled to fit within the limits of the figure.

The anion/cation photoelectron signal predicted from the density profile of the classical MD simulation is shown in Figure 3 as a solid line. Theoretical ion densities are converted into simulated XPS atomic ratios using the convolution integral,

$$S(K.E.) \sim \int e^{\frac{-z}{\Gamma(KE)}} \rho(z) dz$$

for each ion, where z is the distance into the sample from the aqueous vapor interface, ρ(z) is the ion density as a function of depth into solution, obtained from the results of the MD simulation, and Γ(KE) is the IMFP of the photoelectrons as they exit the sample. The experimental IMFP values of Ottosson[19] determined for neat liquid water have been used in these calculations. The experimental results are in good qualitative agreement with the classical MD simulation when integrated over the exponentially decaying probe depth that is characteristic of this APPES experiment. That is, both the experiments and the classical MD simulation exhibit an anion/cation atomic ratio of unity (within the present precision of the experiment) throughout the interfacial region to a maximum probe depth of 2 nm.

Previous measurements of the anion/cation atomic ratios throughout the interfacial region of saturated solutions of KBr and KI are shown in Figure 5,[17] overlaid with the current results of the 6 M KF aqueous solution. These results were collected in a

similar multi-depth APPES experiment as those presented herein. The current study provides experimental validation of the stark contrast between the surface propensity of soft/large versus hard/small halide ions predicted by JT's classical MD simulations[6] (see Figure 1). Significant interfacial anion enhancement was observed at low photoelectron kinetic energies (150 eV) in the saturated KBr and KI solutions, while the bulk 1.0 (±0.1) ratios were recovered at high photoelectron kinetic energies (Figure 5). These results were the first direct experimental validation of the theoretical predictions of JT. In the current study of a 6 M KF electrolyte solution there is no preferential segregation of fluoride to the aqueous-vapor interface at any of the depths probe in this study. The atomic ratio of fluoride to potassium remains unity to a depth of 2 nm in a 6 M aqueous solution of KF.

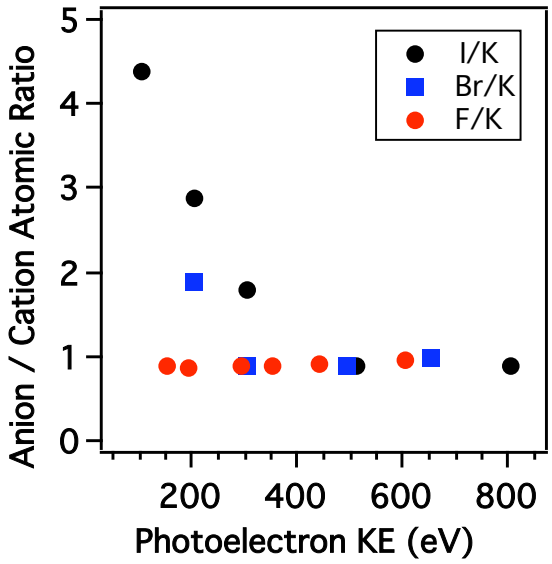

Figure 5: Experimentally measured anion/cation atomic ratios as a function of photoelectron kinetic energy for saturated solutions of KBr and KI (previous study by Ghosal et al.)[17] and the current 6 M KF solution of this study.

Changes of surface potential with composition of the solution can be measured and, when extrapolated to infinite dilution, afford $\Delta\chi$ = χ(solution) - χ(neat water),[22] which provides insight into the changes of the structure of the aqueous-vapor interface upon addition of electrolyte. The values of $\Delta\chi$ are generally positive for alkali solutions of halide salts, *i.e.* KCl, KBr, and KI, and this has been interpreted as being indicative of an ionic double layer near the surface with its negative side (anion) pointing toward the

vapor and its positive side (cation) pointing toward the bulk solution.[22] The exception is KF, which exhibits a negative $\Delta\chi$, albeit with a relatively small magnitude which suggests that the ions are well mixed in the interfacial region, with a slightly closer approach of the potassium toward the surface. Results from Ghosal et al.[17] using multi-depth APPES have confirmed the presence of an electric double layer in saturated solutions of KBr and KI. The present study suggests a slightly closer approach of the potassium ion to the interface (F^-/K^+ atomic ratio of 0.90 at 150 eV and 0.97 at 600 eV), however the results are within the present precision of this experiment and point to the ions (both potassium and fluoride) being well mixed within the interfacial region of 6 M KF to a depth of 2 nm.

Both the APPES experiments and the force field-based MD simulation consistently reveal the lack of anion enhancement at the air-solution interface of a concentrated KF solution. Moreover, the MD simulation predicts that fluoride anions are repelled from the solution-air interface, such that there is an ion-free region a few Ångstroms wide near the surface of the solution (see Figure 4). The repulsion of the fluoride anion from the air-water interface has been further supported by a calculation of the potential of mean force for transporting a fluoride anion across the air-water interface using first principles MD simulations, in which the potential and forces are computed via the electronic structure via density functional theory. The results depicted in the lower panel of Figure 6 show that the potential of mean force (PMF) for moving the fluoride ion in the direction normal to the interface is flat from the interior of the water slab ($z < 0$) until the Gibbs dividing surface is reached. Above the Gibbs dividing surface ($z > 0$) the PMF rapidly increases with increasing z, indicating that the ion is repelled from the surface of the solution. The lack of a minimum in the PMF in the interfacial region is consistent with the absence of an enhancement of the fluoride anion at the interface revealed by the APPES data and results from the force field-based MD simulation.

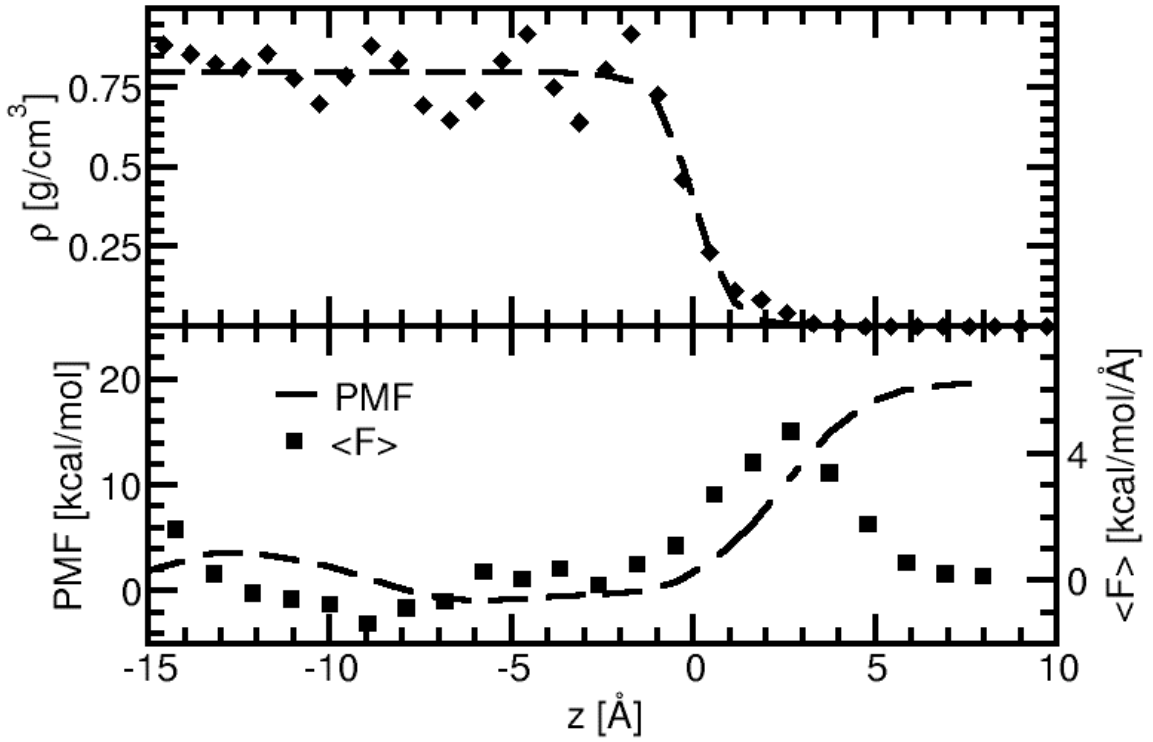

Figure 6: (Top) Density profile of water from first principles molecular dynamics (filled diamonds) fitted to $\rho(z)=0.5\rho_l[1-\tanh((z-z_{GDS})/\delta)]$ *(dashed line). The bulk density,* $\rho_l \approx 0.80\ g/cm^3$*, is consistent with previous results obtained using a similar potential and different simulation protocols.[23] The Gibbs dividing surface, taken here to be the position at which the water density is half its bulk value, has been shifted to z = 0. (Bottom) The potential of mean force (dashed line, left scale), obtained by integrating the average force profile (filled squares, right scale).*

Experimental: The APPES instrument is located at beamline 11.0.2 of the Advanced Light Source (ALS) at Lawrence Berkeley National Laboratory (LBNL). This apparatus has been described in detail elsewhere.[24, 25] Here, two differences from traditional XPS that enable depth profiling of ions at liquid interfaces are described. First, beamline 11.0.2 at the ALS provides synchrotron radiation with a tunable energy in the range of 75-2200 eV. Varying the energy of the ejected photoelectrons by carrying out experiments as a function of x-ray wavelength generates a depth profile of the aqueous-vapor interfacial region. Second, the three differential pumping stages of the electrostatic transfer lens allow ultrahigh vacuum characterization of the photoelectrons while the sample is exposed to Torr-level pressures. In addition, the differentially pumped lens system minimizes the path length of the photoelectrons in the high-pressure region of the chamber and therefore reduces the effects of inelastic scattering of electrons

by gas molecules. The differentially pumped electrostatic lens permits the APPES sampling region to be outfitted with a liquid micro-jet source in contact with its equilibrium vapor pressure.

The setup of the liquid micro-jet has been described in a separate publication.[26] Two unique aspects of XPS from a liquid micro-jet source that facilitate these studies are presented. First, the liquid micro-jet provides a continuously refreshed interfacial region that is exchanged rapidly enough to remain contamination-free (in particular, free of hydrocarbons) and shows no signs of beam-induced halide damage. Second, the liquid micro-jet provides a means to study aqueous saline solutions at concentrations below saturation. Combining a liquid micro-jet with the APPES experiment enables explorations heretofore impossible with in the previous experimental approach that relied on the deliquescence of a solid single crystal to produce a saturated solution.

A 75 μm liquid micro-jet of 6 molar potassium fluoride (Sigma Aldrich, ACS reagent, 99^{+}%) was passed directly in front of the entrance aperture to the differentially pumped electrostatic transfer lens of the kinetic energy analyzer. The liquid micro-jet remains collimated without breaking up into free droplets in the sampling region (about 3 cm from the orifice where the micro-jet is generated). The temperature of the collected liquid is held at -9 °C, *i.e.* the background vapor pressure in the chamber is 2.75 Torr. The jet is irradiated by incident photons of variable energy and the F(1s), K(2p), and O(1s) spectra are recorded. For each core level, the incident radiation is tuned (Table 1) to generate photoelectrons with kinetic energies of 150, 190, 300, 350, 440 and 600 eV. The depth-dependent F^{-}/K^{+} atomic ratio was determined from the F(1s) and K(2p) spectra. An F^{-}/K^{+} sensitivity factor was determined experimentally for each kinetic energy by measuring F(1s) and K(2p) spectra on a dry, freshly cleaved KF single crystal sample with a nominal F^{-}/K^{+} atomic ratio of 1. The ratio of the F(1s)/K(2p) peak areas from the solution were then normalized by the experimentally determined sensitivity factor, yielding the F^{-}/K^{+} atomic concentration as a function of photoelectron kinetic energy.

Molecular dynamics simulations: Molecular dynamics simulations were performed on a 6 molar KF aqueous solution system using the AMBER 8 suite of codes[27] with polarizable force fields.[28, 29] The force field for the fluoride ion was from Markovich

et al.[30] and the potassium ion from Chang and Dang.[31] Water molecules were modeled using the POL3[32] potential. In order to model the liquid-vapor interface the systems were arranged in a slab configuration.[33, 34] The system considered here consisted of 864 water molecules and 96 K^+ and F^- ions. The slab was placed into a 30 x 30 x 100 $Å^3$ rectangular box and three-dimensional periodic boundary conditions were applied. The dynamics were run at 300 K in the weak coupling ensemble.[35] The smooth particle mesh Ewald method[36] was used to compute the electrostatic interactions, and the van der Waals interactions and the real space part of the Ewald sum were truncated at 12 Å. Results shown in this manuscript are from a 2 ns long trajectory following 1 ns of equilibration.

To test the accuracy of the particular combination of force field parameters used here, the density of a bulk solution of 5.3 weight percent KF in water was computed from a constant temperature and pressure MD simulation. The simulation accurately reproduced the value reported in the literature[37] to within 1% (i.e., $\rho_{computed}$ (300 K) = 1.048 g/cm^3 vs. $\rho_{literature}$ (298 K) = 1.0365 g/cm^3).

First principles molecular dynamics simulations: The potential of mean force (PMF) for fluoride ion transport across the air-water interface water was constructed using a series of 26 first principles molecular dynamics simulations (FPMD) in which the fluoride anion was constrained at a series of 1.06 Å intervals as a function of interfacial depth. The PMF was obtained by integrating the profile of the average of the z-component of the force on the fluoride ion constructed from the 26 simulations. Each FPMD simulation was carried out with the simulation code CP2K[38, 39] using a potential based on the Kohn-Sham formulation of density functional theory with BLYP exchange and correlation functionals.[40, 41] The potential was computed using a triple zeta basis set with double polarization (TZV2P) Gaussian type orbitals, and an auxiliary plane wave basis set expanded up to 280 Ry for the valence states, which has been shown to provide accurate energies and forces for MD simulations.[39] The core states were described by GTH pseudopotentials.[42] Forces were obtained after the energy had converged to a tolerance of 10^{-7} H. The initial configurations were prepared from previously equilibrated water slab configurations[23, 43] by substituting a single water molecule in the slab with a fluoride ion at the desired interfacial depth. For simulations in which the fluoride anion was outside the water slab, restrained dynamics was performed to obtain the initial

configurations. Each simulation contained 215 water molecules and a single fluoride anion in a simulation box of 15 x 15 x 71.44 $Å^3$. All of the simulations were performed at 300 K in the NVT ensemble using "massive" Nosé-Hoover chains[44, 45] coupled to every degree of freedom with a time constant of 100 fs. Each simulation consisted of 2 ps equilibration and a production run of 4 to 6 ps. It has been shown elsewhere that structural and dynamical properties of air-water interface as computed via FPMD simulations are in agreement with experiments,[23, 43] despite the failure to predict correctly the bulk density of liquid water.[46]

Conclusions: By coupling a liquid micro-jet of 6 M KF with an APPES experiment the first depth profile into a sub-saturated aqueous solution of KF has been collected. The liquid jet provides a continuously refreshed interface that is devoid of carbonaceous impurities that have been previously reported for similar systems under static conditions.[17, 47] Kinetic energy-dependent depth profiling allows for the anion to cation atomic ratio to be determined throughout the interfacial region to a depth of 2 nm. The F^-/K^+ atomic ratio of a 6 M aqueous KF solution remains stoichiometric, within the present precision of the experiments, throughout the entire interfacial region. The experimental results are in good qualitative agreement with the results of a classical MD simulation of the same system when integrated over an exponentially decaying probe depth that is characteristic of an APPES experiment. Together these results provide a detailed description of the interfacial region of alkali fluoride systems that was previous missing in the literature. The results presented herein, and those reported by this group previously on saturated solutions of KI and KBr,[17] have now quantitatively established the difference in surface propensity of large/soft and small/hard halide ions in aqueous solution.

Acknowledgements: The authors thank Ed Wong and Dr. Kevin Wilson for their assistance with equipment design and setup at the beamline. The AirUCI Environmental Molecular Sciences Institute supported this work under grant CHE 0431312 from the National Science Foundation. The ALS and the molecular environmental sciences beamline (11.0.2) are supported by the Director, Office of Science, Office of Basic Energy Sciences, Division of Chemical Sciences, Geosciences, and Biosciences and Materials Sciences Divisions of the U.S. Department of Energy at the LBNL under

contract DE-AC02-76SF00098. MAB acknowledges the ALS for the Doctoral Fellowship. Computer time for the first principles molecular dynamics simulations was provided by Livermore Computing, and was performed under the auspices of the U.S. Department of Energy by Lawrence Livermore National laboratory under Contract DE-AC52-07NA27344.

Photoelectron Kinetic Energy	F(1s) Photon Energy	K(2p) Photon Energy	O(1s) Photon Energy
150 eV	838 eV	450 eV	690 eV
190 eV	878 eV	490 eV	730 eV
300 eV	988 eV	600 eV	840 eV
350 eV	1038 eV	650 eV	890 eV
440 eV	1128 eV	740 eV	980 eV
600 eV	1288 eV	900 eV	1140 eV

Table 1: Summary of incident photon energies.

References

1. J. H. Hu, Q. Shi, P. Davidovits, D. R. Worsnop, M. S. Zahniser and C. E. Kolb, *Journal of Physical Chemistry*, 1995, **99**, 8768-8776.
2. L. X. Dang, J. E. Rice, J. Caldwell and P. A. Kollman, *Journal of the American Chemical Society*, 1991, **113**, 2481-2486.
3. L. Perera and M. L. Berkowitz, *Journal of Chemical Physics*, 1991, **95**, 1954-1963.
4. L. Vrbka, M. Mucha, B. Minofar, P. Jungwirth, E. C. Brown and D. J. Tobias, *Current Opinion in Colloid & Interface Science*, 2004, **9**, 67-73.
5. P. Jungwirth and D. J. Tobias, *Journal of Physical Chemistry B*, 2002, **106**, 6361-6373.
6. P. Jungwirth and D. J. Tobias, *Journal of Physical Chemistry B*, 2001, **105**, 10468-10472.
7. P. Jungwirth and D. J. Tobias, *Chemical Reviews*, 2006, **106**, 1259-1281.
8. D. J. Tobias and J. C. Hemminger, *Science*, 2008, **319**, 1197-1198.
9. R. Weber, B. Winter, P. M. Schmidt, W. Widdra, I. V. Hertel, M. Dittmar and M. Faubel, *Journal of Physical Chemistry B*, 2004, **108**, 4729-4736.
10. B. Winter, R. Weber, P. M. Schmidt, I. V. Hertel, M. Faubel, L. Vrbka and P. Jungwirth, *Journal of Physical Chemistry B*, 2004, **108**, 14558-14564.
11. P. B. Petersen and R. J. Saykally, *Chemical Physics Letters*, 2004, **397**, 51-55.
12. P. B. Petersen and R. J. Saykally, *Journal of Physical Chemistry B*, 2006, **110**, 14060-14073.
13. P. B. Petersen and R. J. Saykally, *Annual Review of Physical Chemistry*, 2006, **57**, 333-364.
14. P. B. Petersen, R. J. Saykally, M. Mucha and P. Jungwirth, *Journal of Physical Chemistry B*, 2005, **109**, 10915-10921.
15. D. F. Liu, G. Ma, L. M. Levering and H. C. Allen, *Journal of Physical Chemistry B*, 2004, **108**, 2252-2260.
16. E. A. Raymond and G. L. Richmond, *Journal of Physical Chemistry B*, 2004, **108**, 5051-5059.
17. S. Ghosal, J. C. Hemminger, H. Bluhm, B. S. Mun, E. L. D. Hebenstreit, G. Ketteler, D. F. Ogletree, F. G. Requejo and M. Salmeron, *Science*, 2005, **307**, 563-566.
18. W. E. Morgan, W. J. Stec and J. R. Vanwazer, *Journal of the American Chemical Society*, 1973, **95**, 751-755.
19. N. Ottosson, Goteborg University, 2007.
20. R. W. Boyd, *Nonlinear Optics*, 2nd edn., Elsevier, Amsterdam, The Netherlands, 2003.
21. Y. R. Shen, *The Principles of Nonlinear Optics*, Wiley, New York, 1984.
22. J. E. B. Randles, *Physics and Chemistry of Liquids*, 1977, **7**, 107-179.
23. I. F. W. Kuo and C. J. Mundy, *Science*, 2004, **303**, 658.
24. D. F. Ogletree, H. Bluhm, G. Lebedev, C. S. Fadley, Z. Hussain and M. Salmeron, *Review of Scientific Instruments*, 2002, **73**, 3872-3877.
25. H. Bluhm, K. Andersson, T. Araki, K. Benzerara, G. E. Brown, J. J. Dynes, S. Ghosal, M. K. Gilles, H. C. Hansen, J. C. Hemminger, A. P. Hitchcock, G.

Ketteler, A. L. D. Kilcoyne, E. Kneedler, J. R. Lawrence, G. G. Leppard, J. Majzlam, B. S. Mun, S. C. B. Myneni, A. Nilsson, H. Ogasawara, D. F. Ogletree, K. Pecher, M. Salmeron, D. K. Shuh, B. Tonner, T. Tyliszczak, T. Warwick and T. H. Yoon, *Journal of Electron Spectroscopy and Related Phenomena*, 2006, **150**, 86-104.

26. D. E. Starr, E. K. Wong, D. R. Worsnop, K. R. Wilson and H. Bluhm, *Physical Chemistry Chemical Physics*, 2008, DOI: 10.1039/b800717a
27. D. A. Case, T. E. Darden, T. E. I. Cheatman, C. L. Simmerling, J. Wang, R. E. Duke, R. Luo, K. M. Merz, B. Wang, D. A. Pearlman, M. Crowley, S. Brozell, V. Tsui, H. Gohlke, J. Mongan, V. Hornak, G. Cui, P. Beroza, C. Schafmeister, J. W. Caldwell, W. S. Ross and P. A. Kollman, University of California, San Francisco, Amber 8, 2004.
28. L. Perera and M. L. Berkowitz, *Journal of Chemical Physics*, 1994, **100**, 3085-3093.
29. J. Caldwell, L. X. Dang and P. A. Kollman, *Journal of the American Chemical Society*, 1990, **112**, 9144-9147.
30. G. Markovich, L. Perera, M. L. Berkowitz and O. Cheshnovsky, *Journal of Chemical Physics*, 1996, **105**, 2675-2685.
31. T. M. Chang and L. X. Dang, *Journal of Physical Chemistry B*, 1999, **103**, 4714-4720.
32. J. W. Caldwell and P. A. Kollman, *Journal of Physical Chemistry*, 1995, **99**, 6208-6219.
33. I. Benjamin, *Journal of Chemical Physics*, 1991, **95**, 3698-3709.
34. M. A. Wilson and A. Pohorille, *Journal of Chemical Physics*, 1991, **95**, 6005-6013.
35. H. J. C. Berendsen, J. P. M. Postma, W. F. Vangunsteren, A. Dinola and J. R. Haak, *Journal of Chemical Physics*, 1984, **81**, 3684-3690.
36. U. Essmann, L. Perera, M. L. Berkowitz, T. Darden, H. Lee and L. G. Pedersen, *Journal of Chemical Physics*, 1995, **103**, 8577-8593.
37. O. Sohnel and P. Novotny, *Densities of aqueous solutions of inorganic substances*, Elsevier, New York, 1985.
38. CP2K, http://cp2k.berlios.de
39. J. VandeVondele, M. Krack, F. Mohamed, M. Parrinello, T. Chassaing and J. Hutter, *Comput. Phys. Commun.*, 2005, **167**, 103.
40. C. Lee, W. Yang and R. G. Parr, *Phys. Rev. B*, 1988, **37**, 785.
41. A. D. Becke, *Phys. Rev. A*, 1988, **38**, 3098.
42. S. Goedecker, M. Teter and J. Hutter, *Phys. Rev. B*, 1996, **54**, 1703.
43. I. F. W. Kuo, C. J. Mundy, B. L. Eggimann, M. J. McGrath, J. I. Siepmann, B. Chen, J. Vieceli and D. J. Tobias, *Journal of Physical Chemistry B*, 2006, **110**, 3738-3746.
44. G. J. Martyna, M. L. Klein and M. Tuckerman, *J. Chem. Phys.*, 1992, **97**, 2635.
45. D. J. Tobias, G. J. Martyna and M. L. Klein, *J. Phys. Chem.*, 1994, **97**, 12959-12966.
46. M. J. McGrath, J. I. Siepmann, I. F. W. Kuo, C. J. Mundy, J. VandeVondele, J. Hutter, F. Mohamed and M. Krack, *Journal of Physical Chemistry A*, 2006, **110**, 640-646.

47. M. J. Krisch, R. D'Auria, M. A. Brown, D. E. Starr, H. Bluhm, D. J. Tobias and J. C. Hemminger, *Journal of Physical Chemistry C*, 2007, **111**, 13497-13509.